lubricants

Article

Experimental Investigation into the Friction Coefficient of Ball-on-Disc in Dry Sliding Contact Considering the Effects of Surface Roughness, Low Rotation Speed, and Light Normal Load

Qi Wen [1], Mingming Liu [1], Zenglei Zhang [2] and Yunyun Sun [1,*]

1 School of Power and Mechanical Engineering, Wuhan University, Wuhan 430072, China
2 Wuhan Second Ship Design and Research Institute, Wuhan 430205, China
* Correspondence: sunyunyun@whu.edu.cn

Abstract: The friction coefficient is one of the key parameters in the tribological performance of mechanical systems. In the condition of light normal load and low rotation speed, the friction coefficients of ball-on-disc with rough surface in dry sliding contact are experimentally investigated. Friction tests are carried out under normal load 2–9 N, rotation speed 20–48 rpm at room temperature, and surface roughness 0.245–1.010 μm produced by grinding, milling, and turning. Results show that the friction coefficient increases first and then becomes stable, in which the running-in and steady-state periods are included. With the growth of normal load and rotation speed, or the decline of surface roughness, the duration and fluctuation of the running-in period verge to reduce. The whole rising slope of the friction coefficient in the running-in period goes up more quickly with the increment of rotation speed, and it ascends more slowly as normal load enlarges. In terms of the steady-state period, the deviation of the friction coefficient shows a dwindling trend when normal load or rotation speed grows, or surface roughness descends. As normal load or rotation speed rises, the value of the friction coefficient rises first and then drops. Additionally, the mean value of the friction coefficient in steady-state is approximately independent of surface roughness.

Keywords: friction coefficient; surface roughness; ball-on-disc contact; dry sliding

check for updates

Citation: Wen, Q.; Liu, M.; Zhang, Z.; Sun, Y. Experimental Investigation into the Friction Coefficient of Ball-on-Disc in Dry Sliding Contact Considering the Effects of Surface Roughness, Low Rotation Speed, and Light Normal Load. *Lubricants* **2022**, *10*, 256. https://doi.org/10.3390/lubricants10100256

Received: 28 August 2022
Accepted: 10 October 2022
Published: 13 October 2022

1. Introduction

Sliding friction, rolling friction, dry friction, boundary friction, and mixed friction widely exist among mechanical transmission parts, such as the transmission gear in wind turbines and the crankshaft pulley and bearing of automobiles. During the start-up and stop-down stage of mechanical systems, or in the operation condition of low speed and heavy load, elements always befall sliding dry friction, which is accompanied by noise, wear, and energy dissipation. As an important parameter of the tribological system, the friction coefficient means the ratio of the tangential friction force and the normal force between contacting bodies. Measuring the sliding dry friction coefficient, the severe degree, and variation of friction behavior can be obtained intuitively in real time. Based on the value of the friction coefficient and its developing tendency, it could be indirectly judged whether the mechanical transmission parts are in a normal working state or not. Therefore, it is an excellent method for daily fault diagnosis.

The traditional point holds that the friction coefficient is constant and independent of the relative motion speed between contacting bodies. In fact, the friction coefficient is time-dependent and affected by many external factors, including normal load, operating speed, surface roughness, etc. [1]. In order to investigate the variation characteristics of the friction coefficient in dry sliding contact, both theoretical and experimental studies have been conducted in recent years. In the field of theoretical research, Yu et al. [2,3] emphasized that ideal contact surfaces were not smooth, but were rough with a large number of asperities and had self-similar characteristics at the microscale level, i.e., were fractal, and therefore the influence of surface topography on the dynamic contact behavior of mechanical systems was significant and could not be neglected. Liang et al. [4] developed a theoretical model to predict the friction behavior of rough fractal surfaces, which revealed the dependence of the friction coefficient on surface roughness and normal load. Wu et al. [5] established a data surrogate model for the friction coefficient based on the experimental data of a wet clutch under different engagement conditions, and then studied the sensitivity of different factors on the friction coefficient and the coupling relationships among the influencing factors. Vukelic et al. [6] presented a novel method for the determination of the kinetic friction coefficient based on the equation of movement of a rigid body along an inclined plane, and found that increasing sliding velocity increased the deviation of friction coefficients. Zhang et al. [7] developed a numerical approach deriving the macroscale friction coefficient from microscale asperity interactions, which demonstrated that the real contact area first decreased and then stabilized with the increment of surface roughness in lubricated line contact. Zhang et al. [8] established a dynamic friction coefficient model based on the friction transmission mechanism of a wet clutch, and confirmed that both surface roughness and normal load mainly affected the value of the initial and midpoint friction coefficient.

In terms of experimental testing, Kraus et al. [9] used sheet metal compression tests to determine the strain and contact-pressure dependent progression of friction values and confirmed that the friction values changed during the forming process. Zhou et al. [10] obtained gear friction coefficients, reduced with an enlargement in rotation speed from 200 rpm to 1200 rpm by a computational inverse technique, which introduced a surrogate model to describe the mapping relationship between the friction coefficients and root stresses using an adaptive radial basis function. Ghatrehsamani et al. [11] found that the fluctuation of the friction coefficient declined with the growth of normal load from 15 N to 40 N at room temperature under a sliding speed of 0.1 m/s for ST37 (ST37 is St 37 Quality Steels, which is the American steel standard). Li et al. [12] explored the tribological behavior of the friction pair composed of 2297 Al-Cu-Li alloy and GCr15 stainless steel ball under dry friction conditions by a ball-on-disk configuration. The results showed that the friction coefficient significantly changed more as the applied normal load ascended from 1 N to 4 N at 400 rpm, and it was stable in the range of 0.5 to 0.6, regardless of the applied normal load when the rotation speed was large. Pan et al. [13] found the interfacial friction coefficient between bonnet tool and workpiece changed with the variety of the tool rotational speed. Galda et al. [14] demonstrated that the friction coefficient of the so-called smooth journal bearing was substantially greater than that of the textured series at small speeds. Xu et al. [15] studied the friction coefficient of alloy steel of HMn58-2 manganese brass and 20CrMo via the pin-disc friction experiments. It was determined that the effect of rotation speed on the friction coefficient was more obvious than the effect of normal load. Xia et al. [16] found the friction coefficient downsized with the enhancement of sliding speed and normal load between the AA6061 aluminum alloy and P20 steel, and the surface scratch rose and deepened with the increase in the normal load. Wang et al. [17] found that the variation of the friction coefficient between DP780 AHSS sheet and cold-worked DC53 tool steel under normal load changed from 100 N to 900 N. It was determined that the friction coefficient tended to be higher first and then was followed by a general descending behavior. By combining the numerical approach and experimental tests, Pei et al. [18] investigated the friction coefficient evolution during sliding wear in a mixed lubricated rolling-sliding contact, and determined that the friction coefficient was a function of time, which dropped rapidly at first and then kept stable with small fluctuations. To the authors' best knowledge, the above works mainly focused on the value of the friction coefficient under high-speed heavy and light loads, while the variations of the friction coefficient with low speed and light load were not yet investigated for dry sliding contact.

This study investigated the effects of operating conditions (low rotation speed, light normal load) and surface morphology on the variation of the friction coefficient for the ball-on-disc in dry sliding contact. In addition, the influences of applied load, rotation speed, and initial surface roughness on the surface morphology of disc samples after testing were analyzed. Variations of the friction coefficient with different operation times include running-in period and steady-state period. To explore the effect of surface roughness on the friction coefficient in two periods, sliding dry friction coefficient between the grinding ball and disc samples produced by grinding, milling, and turning were measured. Effects of the light normal load and low rotation speed on the friction coefficient between the grinding ball and milling disc sample were conducted at room temperature, respectively. Furthermore, detailed views of the contact region (i.e., the intensity layer and 3D images of the friction track) on the disc sample were obtained.

2. Experimental Materials and Methods

2.1. Materials

The method of ball-on-disc dry sliding friction is adopted in this study. The ball is stationary and is in contact with a rotating disc during the whole testing process. The grinding ball is a 440C steel ball with a diameter of 6.35 mm and a hardness of 58 HRC (HRC means the Rockwell Scale of Hardness, part C.), which is one of the hardest stainless steels and is often utilized to manufacture high strength cutting tools. The material of the disc sample is 304 stainless steel with a diameter of 50.8 mm and a thickness of 6.35 mm. Due to the low value of the hardness of the disc sample (304 stainless steel, approximately 17 HRC), which is much lower than 440C steel, the mass reduction almost only occurs on the disc sample, i.e., the wear of the grinding ball is neglected. Similar to the situation outlined in Reference 11, a significant difference in hardness exists between the experimental materials, and material loss is only observed on the disc. The friction tests are conducted at room temperature (25 °C, controlled by an air conditioner) under normal loads of 2 N, 3 N, 4 N, 6 N, 7 N, 8 N, and 9 N, and a rotation speed of 20 rpm, 24 rpm, 28 rpm, 36 rpm, 40 rpm, 44 rpm, and 48 rpm, respectively. To analyze the effect of surface roughness on the friction coefficient, the utilized disc samples are produced by three kinds of machining methods that include grinding, milling, and turning. The constant diameter d of rotation for grinding, milling, and turning samples is 38 mm, which is determined by the dimensions of the grinding ball and disc sample, and the convenience of observation during the experiments. The dimension and images of disc samples processed by different machining methods are shown in Figure 1.

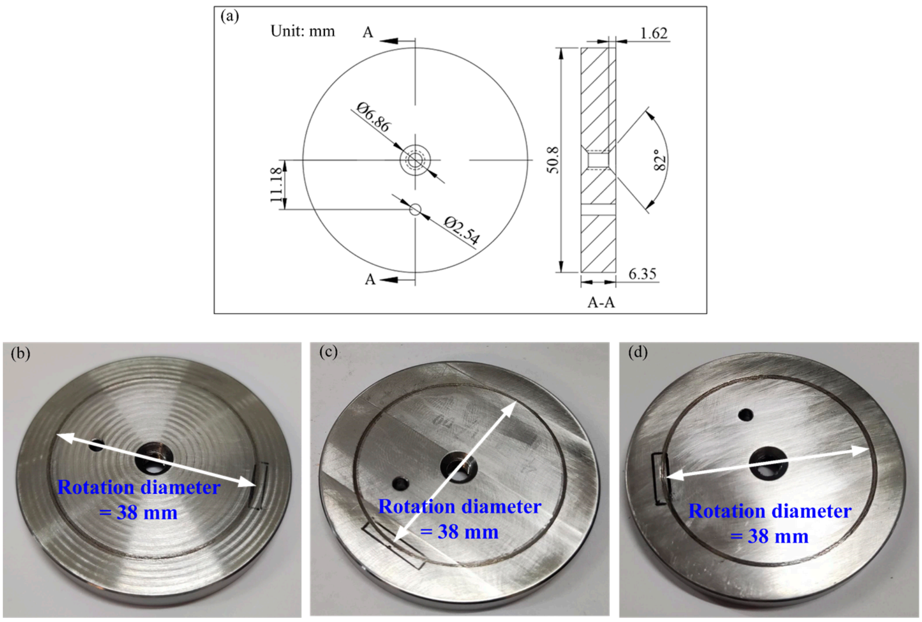

Figure 1. Stainless steel disc samples: (**a**) dimensional information of disc sample; (**b**) turning sample; (**c**) milling sample; (**d**) grinding sample.

2.2. Test Equipment

The friction tests are carried out on a Rtec MFT-5000 universal tribometer (Rtec-instruments, San Jose, CA, USA). It mainly includes the two-dimension force sensor and an integrated system combining control, monitor, and analysis software. The two-dimension force sensor can measure the maximum of 200 N and the minimum of 2 N, both in the x-direction and z-direction, and the rotating module could run from 0.1 rpm to 5000 rpm, with a resolution of 0.1 rpm. The detailed features of experimental instrument are shown in Figure 2a. The instrument can measure the friction coefficient under varying normal loads and rotation speeds for disc samples produced by different machining methods at room temperature, of which the working principle is shown in Figure 2b.

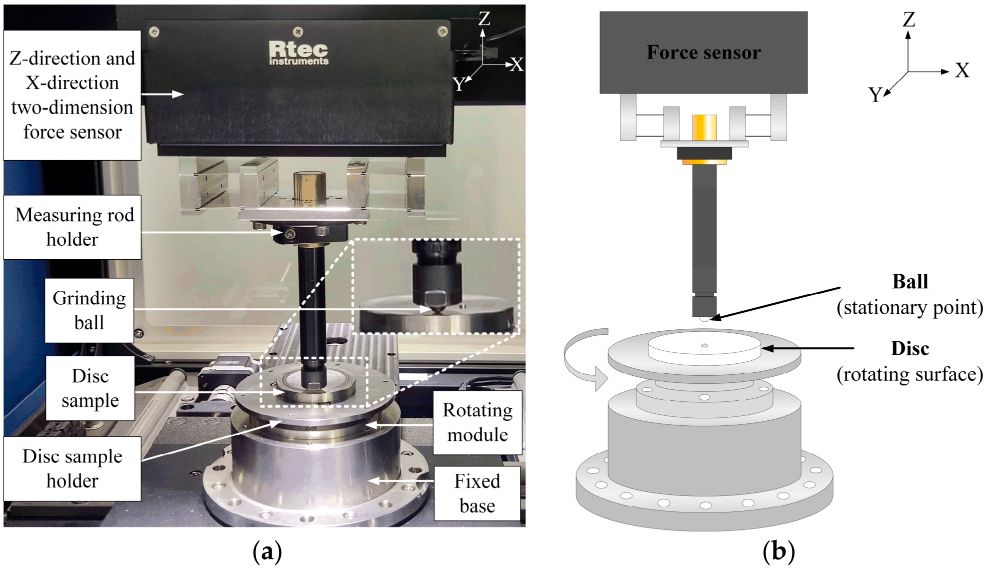

Figure 2. Experimental equipment: (**a**) Rtec MFT-5000 universal tribometer; (**b**) diagram of the friction test equipment.

The grinding ball block remains stationary during the tests, while the rotating module and the 304 stainless steel disc sample keep rotating. The two-dimension force sensor measures the normal load and tangential friction force in real time, transmitting measured data to the computer during the friction process. Meanwhile, the computer automatically calculates the corresponding value of the friction coefficient, and plots simply filtered curves.

2.3. Experimental Arrangement

The friction tests between 440C steel and 304 stainless steel are carried out under different process parameters, including applied normal load and rotation speed. Furthermore, the effect of surface roughness on the friction coefficient is considered. The sliding velocity can be expressed as v(m/s) = [$\pi \cdot d$ (mm)$\cdot n$ (rpm)]/60, where d and n are the diameter of rotation and rotation speed, respectively.

The surface roughness of the disc sample processed by diverse machining methods is weighted by the average value of asperity heights R_a in this work, which could be detected by a NanoFocus 700138 µscan select S/M/L (NanoFocus AG, Oberhausen, Germany). A NanoFocus µscan is an optical profilometer for the three-dimensional measurement and analysis of surfaces. It has a robust confocal point sensor for capturing height profiles, topographies, geometries, and roughness, and an extensive surface analysis program which contains the latest industry standard parameters and filter functions. The velocity of the traversing unit is 2.50 mm/s, and the scan direction is bidirectional from west to east. In addition, the resolution of chromatic longitudinal aberration, confocal sensor, and holographic sensor is 1.8 µm, 1 µm, and 25 µm, respectively. In addition, the scanning resolution in the x and y direction is selected as 5 µm. The scanning range of the instrument is set as 5 mm × 5 mm, and the disc surface of grinding, milling, and turning samples is scanned at three different positions, respectively. In addition, surface roughness R_a of the scanning region is read three times in the width direction and length direction, respectively. The scanning positions are near the friction radius. The diagram of scanning regions and measurement positions of R_a on the disc sample is shown in Figure 3. The measured values of S_a, S_q, S_{ku}, and S_{sk}, and the mean values for disc samples produced by grinding, milling, and turning, are listed in Table 1. The measured values and mean values of R_a for disc samples processed by grinding, milling, and turning are listed in Table 2. The parameters of the operating conditions for friction tests are listed in Table 3.

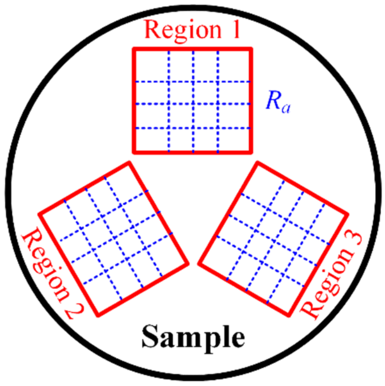

Figure 3. The diagram of scanning regions and measurement positions of R_a on the disc sample.

Table 1. ISO 25178 standard surface texture characterization of disc samples.

Machining Method	ISO 25178 Standard Parameter	Region 1	Region 2	Region 3	Mean	Deviation
Turning	Arithmetical mean height of surface (S_a/µm)	1.69	1.60	1.63	1.64	0.046
	Root mean square height of surface (S_q/µm)	2.06	1.94	1.97	1.99	0.062
	Skewness of surface (S_{sk})	−0.202	−0.341	−0.372	−0.305	0.091
	Kurtosis of surface (S_{ku})	2.76	2.59	2.55	2.633	0.112
Milling	S_a/µm	1.01	0.852	1.12	0.994	0.135
	S_q/µm	1.23	1.02	1.30	1.183	0.146
	S_{sk}	−0.577	−0.299	0.134	−0.247	0.358
	S_{ku}	2.76	2.54	2.07	2.457	0.352
Grinding	S_a/µm	0.468	0.380	0.393	0.414	0.048
	S_q/µm	0.602	0.482	0.496	0.527	0.066
	S_{sk}	−0.346	0.501	−0.027	0.043	0.428
	S_{ku}	5.18	37.9	3.23	15.437	19.478

Table 2. Surface roughness R_a of disc samples processed by grinding, milling, and turning.

Machining Method	Region 1	Region 2	Region 3	Mean Value of Surface Roughness R_a (µm)	Deviation of Surface Roughness R_a (µm)
Turning	1.24	1.08	0.861	1.010	0.173
	1.22	1.06	0.617		
	1.01	1.03	0.898		
	1.18	0.73	1.04		
	1.14	0.905	1.05		
	1.21	0.832	1.07		
Milling	1.08	0.665	0.948	0.781	0.241
	0.87	0.867	1.24		
	0.5	0.981	0.872		
	0.854	0.451	0.85		
	0.850	0.456	0.757		
	0.89	0.288	0.631		
Grinding	0.331	0.218	0.174	0.245	0.068
	0.347	0.181	0.175		
	0.326	0.228	0.202		
	0.326	0.223	0.192		
	0.325	0.206	0.186		
	0.359	0.231	0.182		

Table 3. The parameters of operating conditions.

Normal Load (N)	Rotation Speed (*n*/rpm)
2	20
3	24
4	28
6	36
7	40
8	44
9	48

3. Results and Discussion

3.1. Effects of Surface Roughness on Friction Coefficient

Under the rotation speed of 30 rpm and the normal load of 4 N, the friction coefficient between the 440C steel and 304 stainless steel is recorded at room temperature of ball-on-disc. The data are read for 80 min for the disc sample processed by milling, and the testing time for grinding and turning samples is 40 min. The friction coefficients versus sliding time and sliding distance for three kinds of samples are presented in Figure 4.

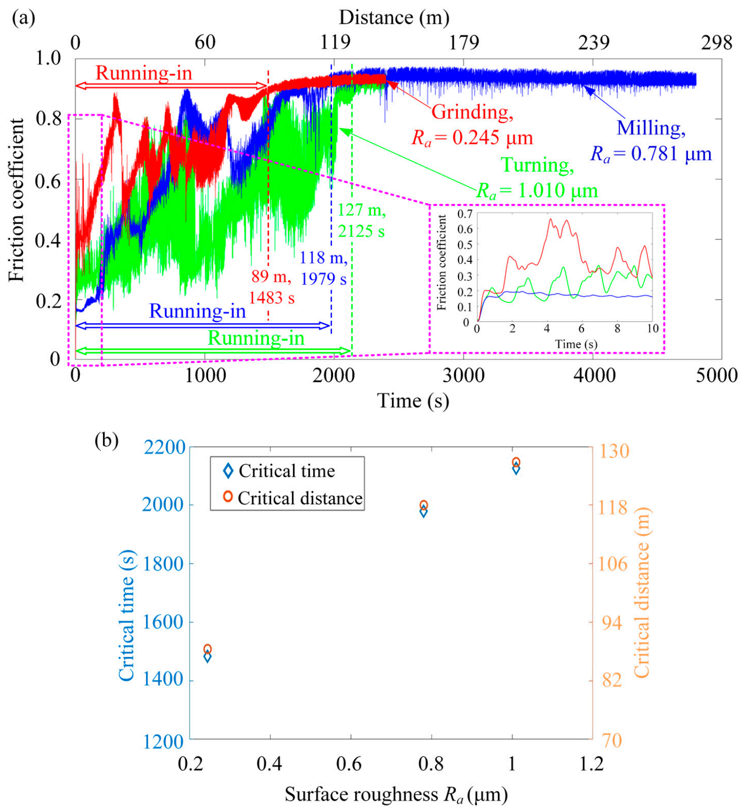

Figure 4. The friction coefficient of disc samples with varying machining methods: (**a**) the evolution of friction coefficient with different surface roughness; (**b**) the critical time and critical distance of friction coefficient vs. surface roughness.

As shown in Figure 4, initially, the friction force rapidly rises. The main reason for this is the conversion from static friction to dynamic friction [16]. Additionally, it can be seen that the friction coefficient of the disc sample always rises and undulates first and then maintains stability. That is because, as time goes by, two fresh surfaces in relative sliding motion begin to experience intimate contact at the asperities level [1], the real contact area between contact bodies keeps increasing; thus, the friction coefficient becomes higher. As the real contact area reaches the maximum value, the friction coefficient remains constant. Generally, the rising period of the friction coefficient is called the running-in, and the stable phase of that is known as the steady-state. In order to compare the duration of running-in under varying normal loads, rotation speeds, and surface roughness more precisely in the study, the critical time when the friction coefficient changes from rising to stable is determined to be 1.12 times the friction coefficient's maximum value during the whole experiment. Specifically, before the critical period, the friction coefficient rapidly increases, and the friction coefficient after the critical period steadily decreases. The friction coefficient after the critical period is larger than the value during the critical period, but is less than 112% of the value at the critical time. The corresponding critical distance is the product of the critical period and the sliding velocity, which could be obtained by rotation speed and rotation diameter.

After the critical period, the tribo-system enters the steady-state period. In order to investigate the value of the friction coefficient during the steady-state under different operating conditions and surface morphologies, both the average value of the friction coefficient in the steady-state period (i.e., the arithmetic mean of friction coefficient recorded from the critical time to the end time), and the fluctuation of friction coefficient during the steady-state (i.e., the standard deviation of friction coefficient measured from the critical time to the end time), are calculated.

Figure 4 shows a comparison of the friction coefficient of disc samples processed by grinding, milling, and turning. The duration and fluctuation of the friction coefficient in the running-in period is proportional to the surface roughness, whereas the value is inversely proportional to the surface roughness. Similar results have been observed in the literature [19–21], which verify the reliability of the experiments in this study. Due to the contact point between the grinding ball and the disc sample, the rougher the surface of sample is in microscale, the more unstable the contact state is; thus, the more obvious the fluctuation of the friction coefficient is. During the running-in, the experimentally measured value of the friction coefficient for the turning sample is overall smaller than that of the other two samples produced by grinding and milling. This phenomenon may be attributed to the following reasons. An increase in surface roughness causes a decrease in the real contact area [22], which means less asperities are involved in contact and experience deformation, so the value of the friction coefficient is correspondingly smaller. With the evolution of friction duration, more asperities become involved in contacting and deforming, and surface profiles get smoother, i.e., surface roughness declines [11], and the friction coefficient value rises. During the running-in period, for the turning sample, of which initial surface roughness is large, the initial value of the friction coefficient is relatively small, and at the same time, the friction coefficient is still smaller than the disc samples made by grinding and milling. Additionally, it can be seen that the smoother the disc sample surface is, the shorter the duration of the running-in period; indicating that friction coefficient transfers to steady-state more easily. Specifically, the turning sample with the surface roughness of 1.010 μm enters the steady-state more slowly, whereas the disc sample processed by grinding with a smoother surface of 0.245 μm enters the steady stage faster than the other cases. The reason for this is because, under the same operating conditions, the maximum real contact area between two bodies is the same, so the average value of the friction coefficient in the steady-state for the three disc samples processed by different machining methods is the same, which means that the value of the steady-state friction coefficient is independent of surface roughness. Therefore, the running-in period of the friction coefficient for the rougher disc sample with a larger initial surface roughness is longer.

Figure 5 shows the average value and standard deviation of the friction coefficient in the steady-state for disc samples processed by different machining methods, with an increment of surface roughness from 0.245 μm to 1.010 μm under the normal load of 4 N and the rotation speed of 30 rpm. For the grinding sample with the surface roughness of 0.245 μm, after the critical period, the friction coefficient is measured 91,700 times. Additionally, the number of measurements for the friction coefficient in the steady-state for the milling sample and the turning sample is 282,100 and 27,500, respectively. The value of the steady-state friction coefficient, whose change is less than 2%, could be regarded as irrelevant to surface roughness, and the fluctuation of that is proportional to surface roughness. As demonstrated, with the growth of the surface roughness from 0.245 μm to 1.010 μm, the steady-state friction coefficient of the disc sample firstly increases by 1.52% from 0.920 to 0.934, and then decreases by 1.82% to 0.917. Meanwhile, the standard deviation of the friction coefficient in the steady-state grows by 28.57% from 0.014 to 0.018. Both of these are explained and analyzed in the previous paragraph. Therefore, the value of the friction coefficient for dry sliding contact is approximately independent of interfacial roughness.

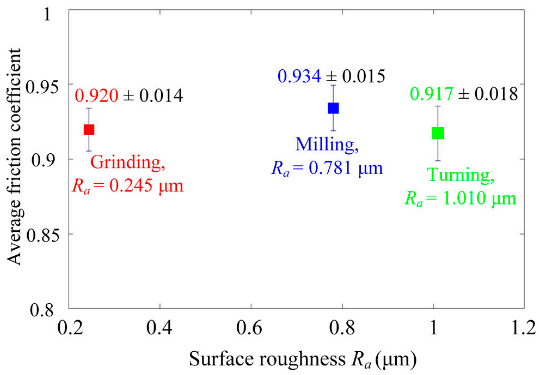

Figure 5. The steady-state friction coefficient of disc samples processed by different machining methods.

Figure 6 shows the 3D image and intensity layer of the contact region (scanning range is 5 mm × 1.3 mm) on disc samples produced by grinding, milling, and turning with 4 N and 30 rpm. The real friction region is a ring, of which the inner and outer edges are marked by a red dotted line on the corresponding intensity layer figure. It is obvious that the smoother the contact surface is, the wider the scratch; i.e., the larger the contact area is. The contact area for the sample with a smaller surface roughness is larger; thus, the duration of the running-in is shorter.

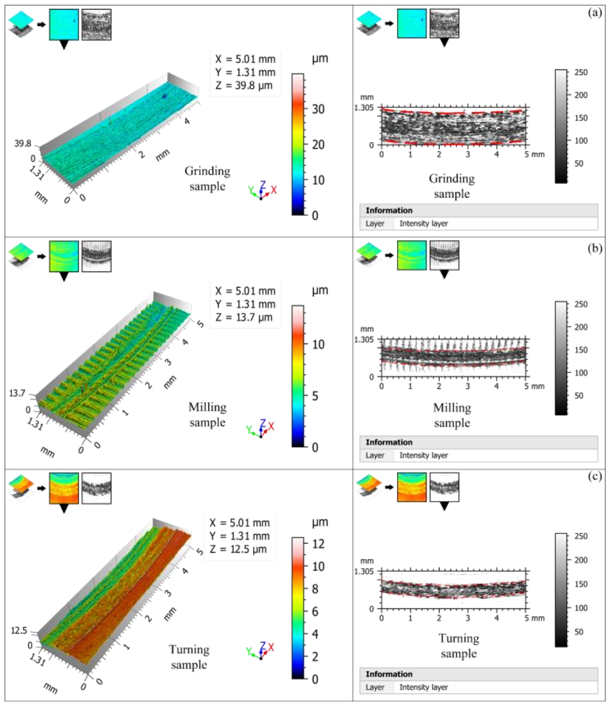

Figure 6. The contact region of disc samples produced by grinding, milling, and turning after friction test under the load of 4 N and the rotation speed of 30 rpm: (**a**) the 3D image and intensity layer of the contact region on the grinding surface; (**b**) the 3D image and intensity layer of the contact region on the milling surface; (**c**) the 3D image and intensity layer of the contact region on the turning surface.

3.2. Effects of Normal Load on Friction Coefficient

Under the rotation speed of 24 rpm and the constant rotation radius of 23.75 mm (i.e., the sliding velocity of 59.69 mm/s), with varying normal loads (2 N, 3 N, 4 N, 6 N, 7 N, 8 N, and 9 N), the friction coefficients are measured between the 440C steel grinding ball and 304 stainless steel milling sample at room temperature. The friction coefficient under 2 N, 3 N, and 4 N is measured for 2 h, and the duration of the friction test under 6 N, 7 N, 8 N, and 9 N is 1 h. The seven variation curves of the friction coefficient vs. sliding time and sliding distance are presented in Figure 7, and indicate that time and normal load affect the friction coefficient.

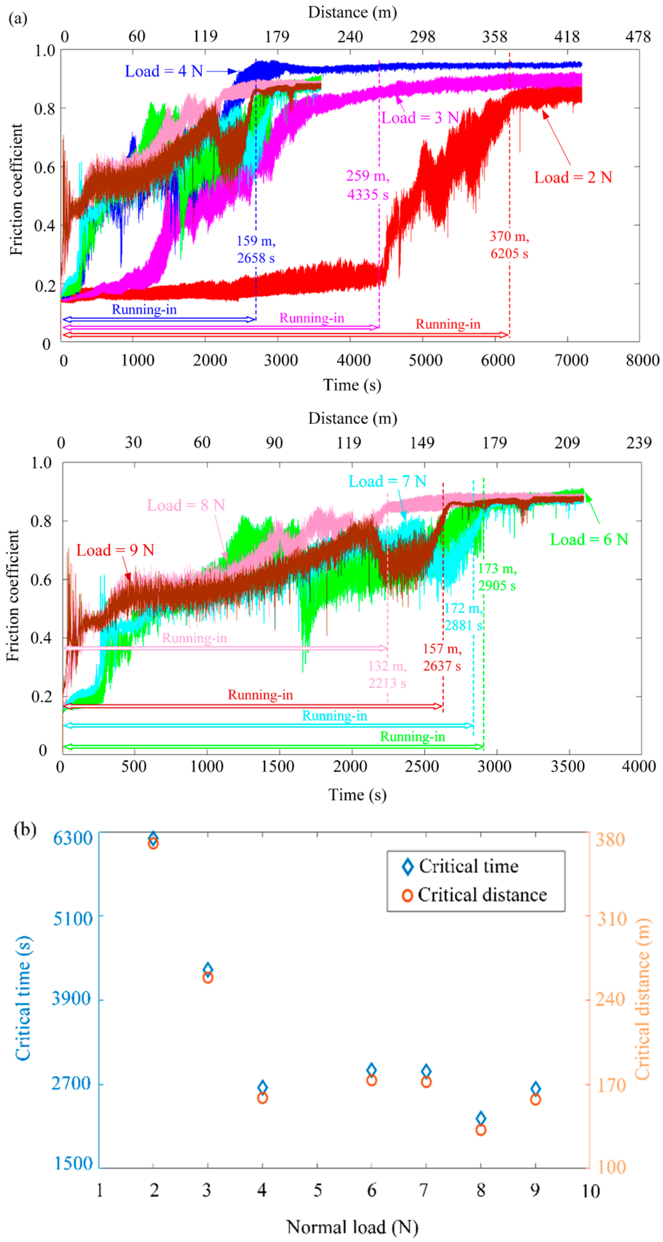

Figure 7. The friction coefficient of milling samples with varying applied loads: (**a**) the evolution of the friction coefficient under different loads; (**b**) the critical time and critical distance of the friction coefficient vs. normal load.

In Figure 7, seven curves of the friction coefficient are presented and compared for 2 N, 3 N, 4 N, 6 N, 7 N, 8 N, and 9 N. It is found that the heavier the normal load is, the lighter the fluctuation and the shorter the duration of the running-in. The fluctuation of the friction coefficient curves is due to real contact surfaces being rough, rather than ideally smooth. Additionally, the variation of contact geometry becomes stable as the applied load grows; hence, the fluctuation of the friction coefficient is reduced. When the normal load goes up from 2 N to 9 N, the critical time (i.e., the duration of running-in) dwindles by 58% from 6205 s to 2637 s. The whole rising slope of the friction coefficient in the running-in rapidly ascends by increasing the applied load from 2 N to 4 N. That is because, when the applied load increases, more asperities on the surface of the disc sample experience contact; therefore, the time it takes for the friction coefficient to achieve stable state decreases and the running-in is increased. When the applied load is 2 N or 3 N, the friction coefficient monotonically increases in the running-in period. When the normal load is 6 N, 7 N, 8 N, or 9 N, the friction coefficient during running-in grows first to 0.8, and then drops to about 0.6,and finally enhances again. As for 4 N, the peak value of the friction coefficient during the running-in is about 0.75 and appears around 1600 s. Under a low applied load, the real contact area between the grinding ball and the surface of the disc sample is small and the adhesion is severe; thus, the friction coefficient is large. The curve of the friction coefficient under 2 N or 3 N represents a dry contact case with the presence of oxidation between the surfaces [1]. Additionally, the curves of the friction coefficient under 4 N–9 N exhibit a peak during the running-in, which can be attributed to the mechanical disruption of surface oxide films and the change of contact geometry. Once the asperities are flattened, the friction coefficient declines [11].

Figure 8 shows the fluctuation of the steady-state friction coefficient is inversely proportional to the applied load, approximately. Under 2 N, after the critical period, the friction coefficient is measured 99,500 times. Additionally, the number of measurements for the friction coefficient in the steady-state under 3 N, 4 N, 6 N, 7 N, 8 N, and 9 N is 286,500, 454,200, 69,500, 71,900, 138,700 and 96,300, respectively. Specifically, the steady-state friction coefficient of disc sample shows an increment of 11.51% from 0.843 to 0.940, and then a wavelike decline by 11.60% from 0.940 to 0.831, with the enlargement of normal load. When the load is relatively small, the plastic ratio significantly increases with an increase in load; thus, the friction coefficient becomes larger [7]. Additionally, as the applied load continues to grow, the contact between metal surfaces with the elastoplastic contact state rises because the asperities are crushed and deformed, resulting in a decrease in the friction coefficient in the steady-state [12]. Furthermore, the standard deviation of the friction coefficient in the steady-state shows a downward trend from 0.021 to 0.011. The reason for which is explained above.

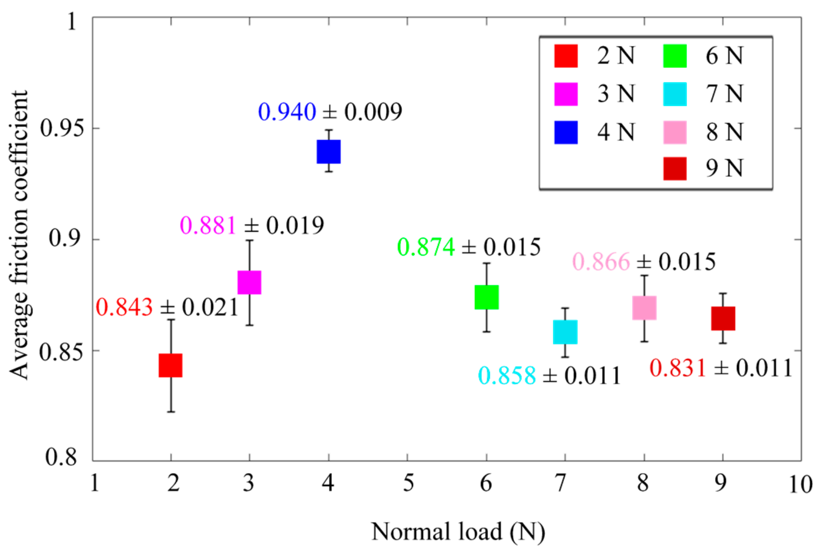

Figure 8. The steady-state friction coefficient of disc samples under varying normal loads.

Figure 9 illustrates the friction scratches on the milling samples with different applied loads and the constant rotation speed of 24 rpm (scanning range is 5 mm × 0.8 mm). With the increment of normal load, the ring width of the friction region is almost constant, but the ratio of low intensity layer in the friction region increases (i.e., the real contact area increases); thus, the friction coefficient enters the steady-state more quickly.

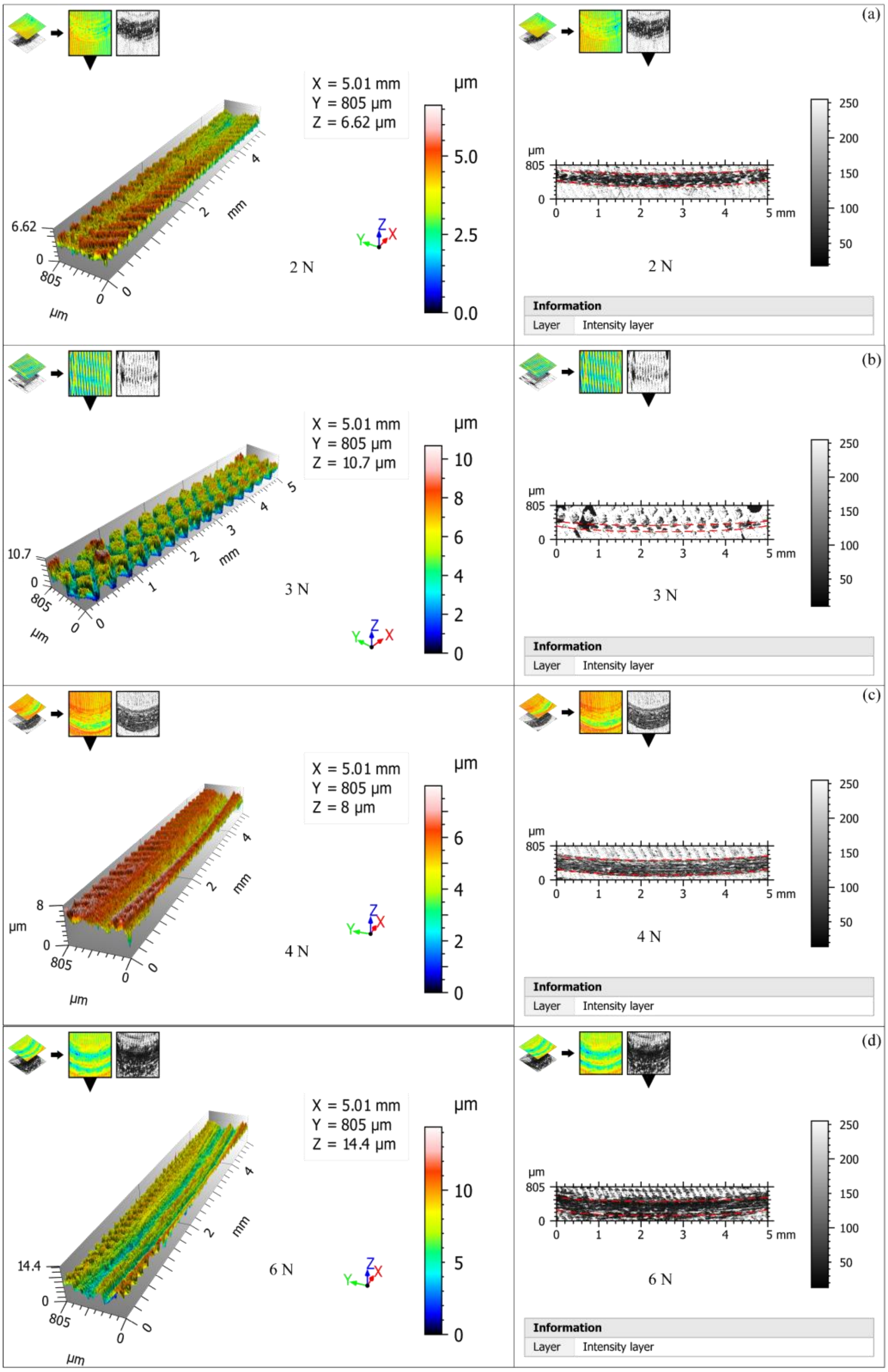

Figure 9. *Cont.*

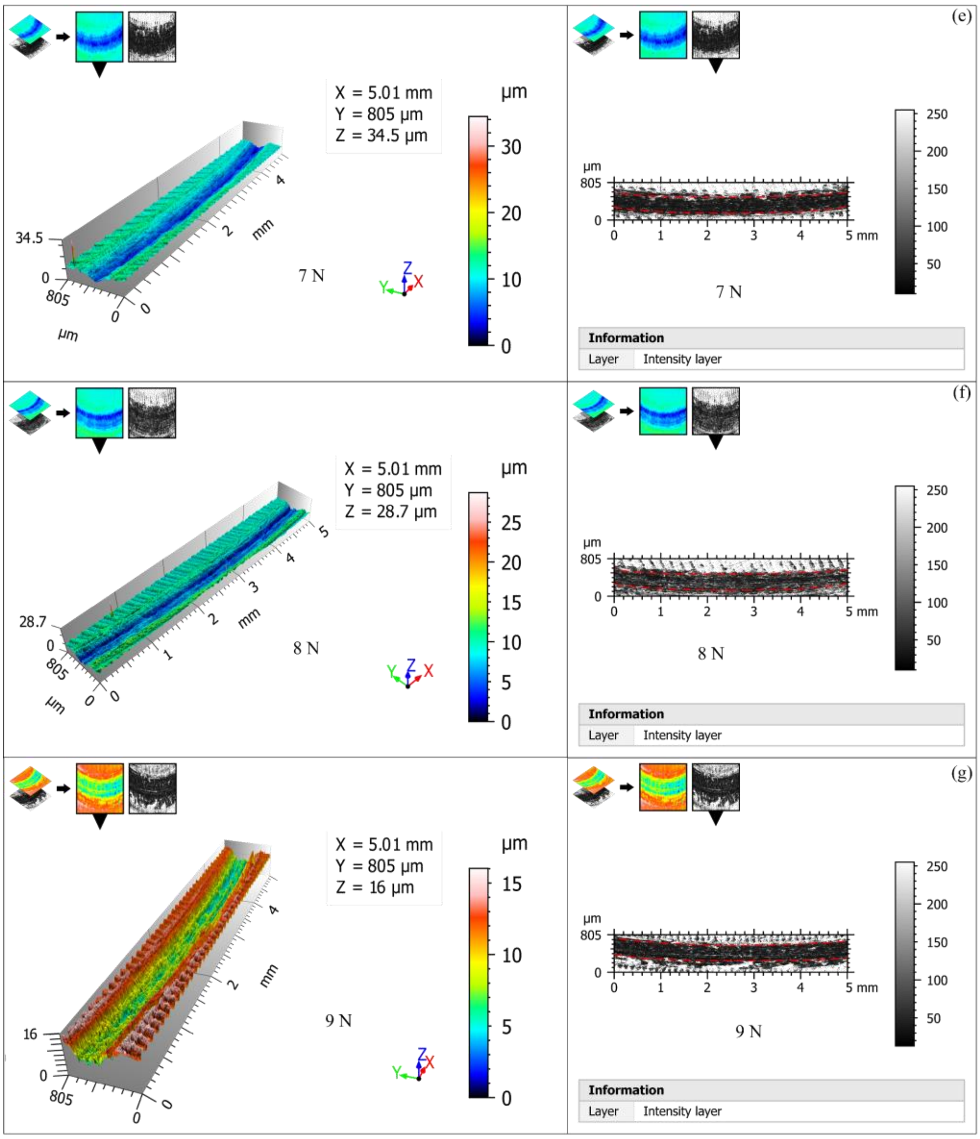

Figure 9. The contact region of the milling sample after friction test under varying loads and the rotation speed of 24 rpm: (**a**) the 3D image and intensity layer of the contact region under 2 N; (**b**) the 3D image and intensity layer of the contact region under 3 N; (**c**) the 3D image and intensity layer of the contact region under 4 N; (**d**) the 3D image and intensity layer of the contact region under 6 N; (**e**) the 3D image and intensity layer of the contact region under 7 N; (**f**) the 3D image and intensity layer of the contact region under 8 N; (**g**) the 3D image and intensity layer of the contact region under 9 N.

3.3. Effects of Rotation Speed on Friction Coefficient

Under the normal load of 4 N and the constant rotation radius of 23.75 mm, at room temperature, the friction coefficients are measured between the 440C steel and 304 stainless steel with varying rotation speeds (20 rpm, 24 rpm, 28 rpm, 36 rpm, 40 rpm, 44 rpm, and 48 rpm) on milling samples. The duration of the friction test under 20 rpm and 24 rpm is 2 h, and the friction experimental time under 28 rpm is 1 h. As for the rotation speed of 36 rpm, 40 rpm, 44 rpm, and 48 rpm, the testing time is 40 min. Friction coefficient versus sliding time is shown in Figure 10.

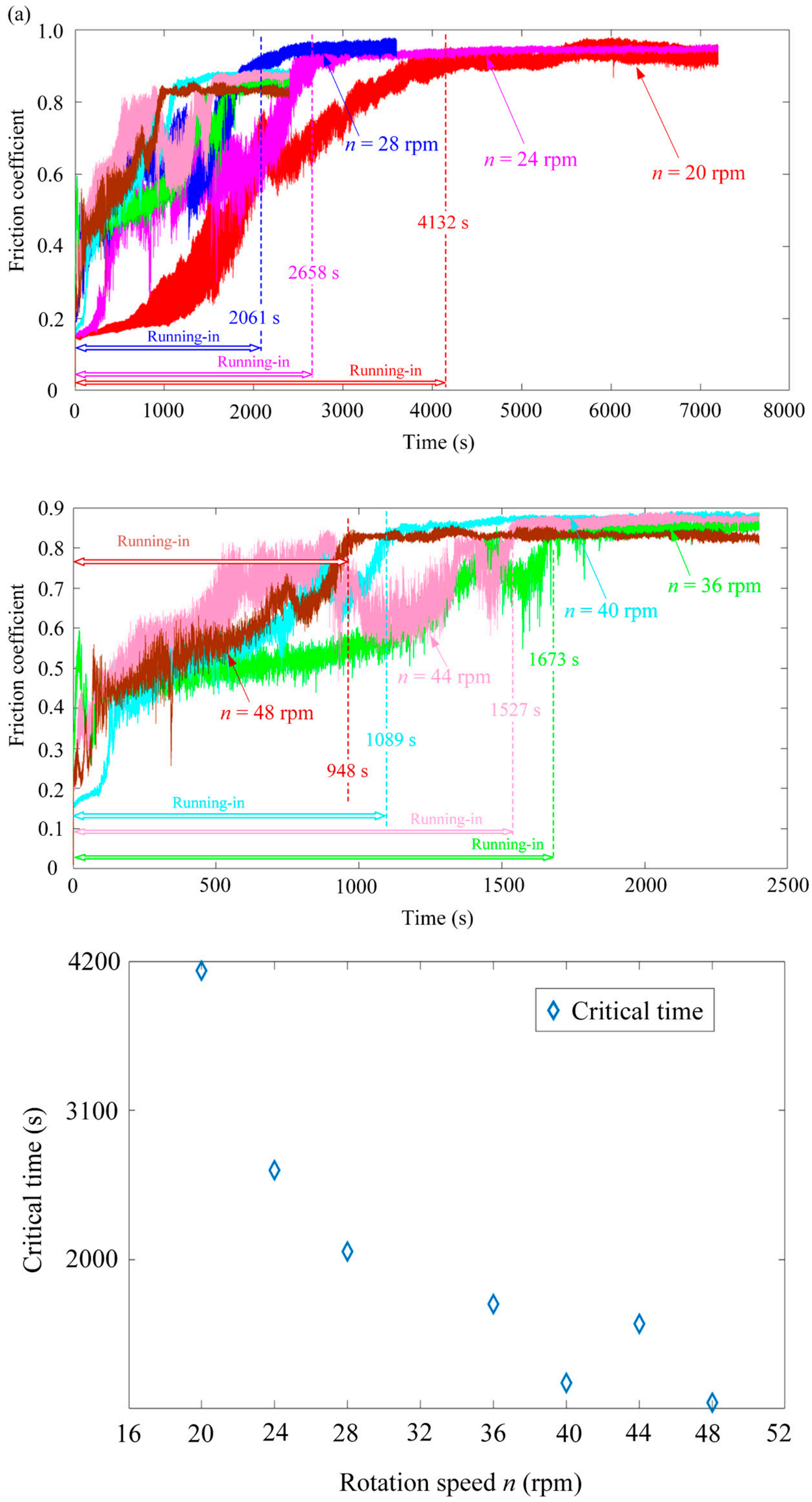

(**b**)

Figure 10. The friction coefficient of milling samples under varying rotation speeds: (**a**) the evolution of friction coefficient under different rotation speeds; (**b**) the critical time of friction coefficient vs. rotation speed.

As Figure 10 shows, the duration and fluctuation of the running-in are inversely proportional to rotation speed, approximately. As expected, during the running-in period, as the rotation speed rises from 20 rpm to 48 rpm, the end time of the running-in period declines by 77.06% from 4132 s to 948 s. Additionally, the whole rising slope of the friction coefficient is larger for a higher rotation speed in the running-in period. Since more asperities are involved in contact, the duration of the running-in decreases and the value of friction coefficient during that time increases with the enhancement of rotation speed. The reason for the appearance of peaks during the running-in when the rotation speed is 20 rpm, 28 rpm, 36 rpm, 40 rpm, 44 rpm, or 48 rpm, is also because the surface oxide films cause mechanical disruption and the asperities are destroyed. Compared with the peak friction coefficient during the running-in period under 48 rpm, the peak for 36 rpm or 40 rpm occurs later with a larger value. This is mainly because increasing the rotation speed causes more asperities to come into contact, but the time for each contact decreases.

Figure 11 shows the average value and deviation of the friction coefficient in the steady-state with the increment of rotation speed from 20 rpm to 48 rpm and the constant normal load of 4 N. Under the rotation speed of 20 rpm, after critical time, the friction coefficient is measured 306,800 times. Additionally, the number of measurements for the friction coefficient in the steady-state under 24 rpm, 28 rpm, 36 rpm, 40 rpm, 44 rpm, and 48 rpm is 454,200, 153,900, 72,700, 131,100, 87,300, and 145,200, respectively. It is obvious that there is an optimal rotation speed value where the friction coefficient is the highest under the normal load of 4 N. Specifically, the steady-state friction coefficient of the disc sample increases by 11.10% from 0.920 to 0.942, with an rise in the rotation speed from 20 rpm to 28 rpm, and then it nonmonotonically decreases by 11.78% to 0.831, from 28 rpm to 48 rpm. Additionally, the fluctuation of the friction coefficient in the steady-state is inversely proportional to rotation speed, approximately. The standard deviation of the friction coefficient in the steady-state drops by 57.89% from 0.019 to 0.008. As the rotation speed rises, the contact area and temperature between the grinding ball and disc sample increase, and the abrasive wear among the asperities gets worse [23], so that the friction coefficient in the steady-state becomes larger. In addition, the shear strain rate increases as rotation speed rises, which causes the contact materials to have greater strength; thus, the real contact area and friction coefficient dwindle [16]. The fluctuation of the friction coefficient reduces growth in the number of contact asperities per unit as the rotation speed increases.

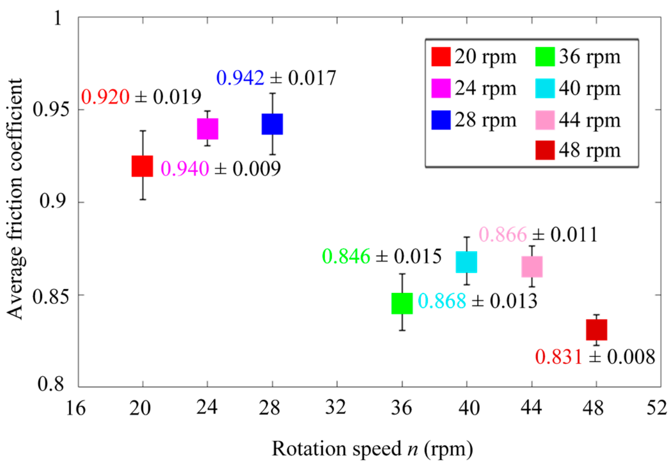

Figure 11. The steady-state friction coefficient of disc samples under different rotation speeds.

Figure 12 shows the intensity layer and 3D image of the friction region (scanning range is 5 mm × 0.8 mm) on the milling samples under a normal load of 4 N and varying rotation speeds. From 20 rpm to 28 rpm, the ring width of the friction region and the ratio of the low intensity layer in the friction region both become larger, which means the contact area and actual contact rate increase; thus, the friction coefficient in the steady-state increases. When rotation speed rises from 28 rpm to 48 rpm, the nominal contact area and the real contact ratio for the friction region decreases and then increases early or late. Therefore, the friction coefficient declines at first, then increases, and finally dwindles again.

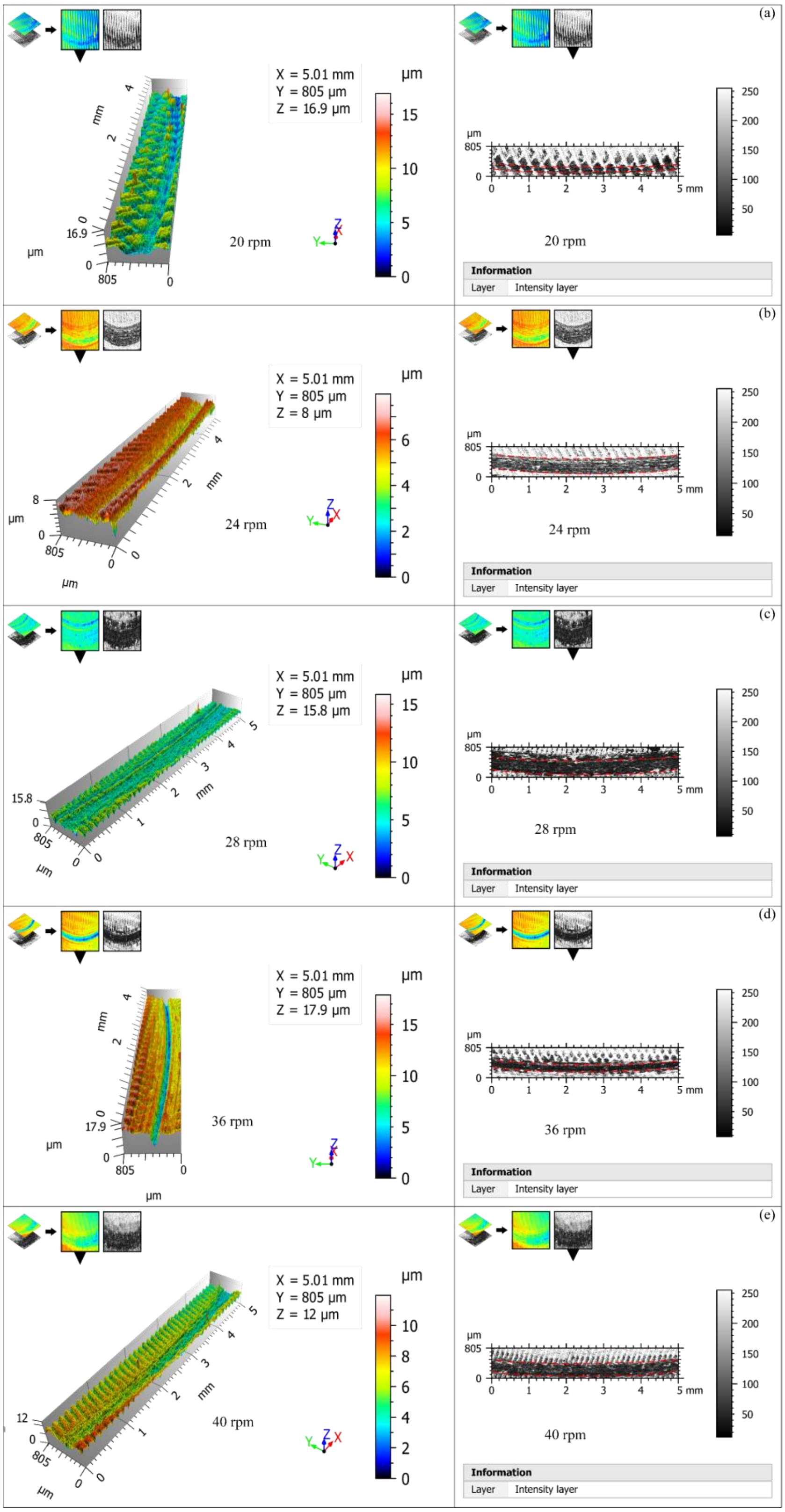

Figure 12. *Cont.*

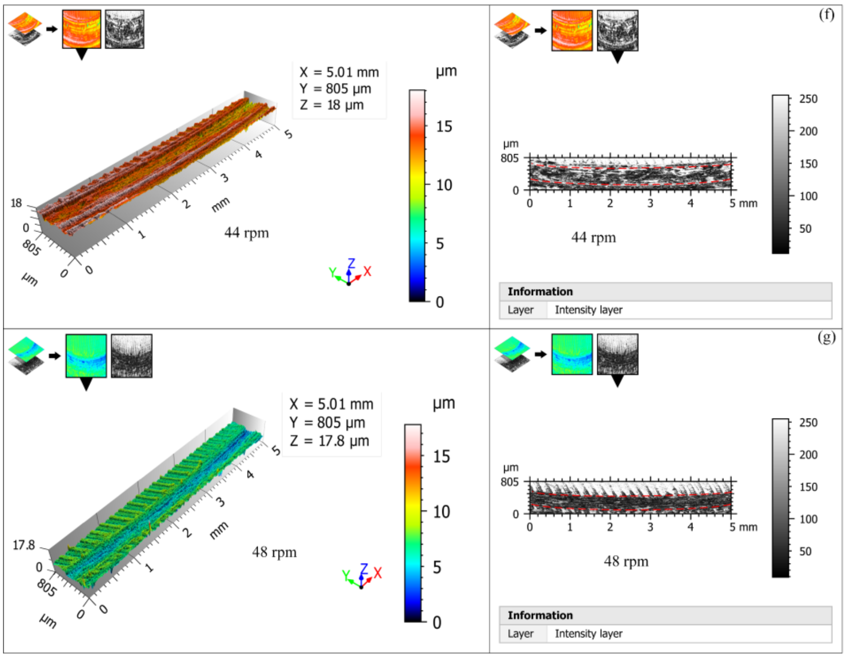

Figure 12. The contact region of the milling sample after friction test under the load of 4 N and varying rotation speeds: (**a**) the 3D image and intensity layer of the contact region under 20 rpm; (**b**) the 3D image and intensity layer of the contact region under 24 rpm; (**c**) the 3D image and intensity layer of the contact region under 28 rpm; (**d**) the 3D image and intensity layer of the contact region under 36 rpm; (**e**) the 3D image and intensity layer of the contact region under 40 rpm; (**f**) the 3D image and intensity layer of the contact region under 44 rpm; (**g**) the 3D image and intensity layer of the contact region under 48 rpm.

4. Conclusions

In this study, friction tests of ball-on-disc in dry sliding contact were conducted. Effects of normal force, rotation speed, and surface roughness on the friction coefficient were experimentally studied in the running-in and steady-state periods. All results were only applicable to the materials, machining methods, and operating conditions in this ball-on-disc study. The detailed conclusions are as follows:

During the running-in period, the heavier the normal load, the higher the rotation speed, and the smoother contact surface corresponds to a larger friction coefficient. Meanwhile, the fluctuation of the running-in becomes smaller as the normal load or rotation speed increases, or as surface roughness decreases. The critical period is inversely proportional to normal load and rotation speed, approximately; whereas it is proportional to surface roughness. In the steady-state period, the friction coefficient tends to be larger at first and then smaller with the increment of normal load or rotation speed. Compared with normal load and rotation speed, surface morphology could be regarded as independent of the friction coefficient during the steady-state. Furthermore, the fluctuation of the steady-state friction coefficient shows a tendency to decrease with and increasing normal load or rotation speed, or decreased surface roughness. And the smoother the surface, the larger the ring width of the friction region. With the increment of normal load, the real contact area increases. By increasing the rotation speed, the ring width and the real contact rate of the friction region show a tendency to increase first, then decrease, and then grow again.

Author Contributions: Conceptualization, Q.W. and Y.S.; data curation, Q.W., M.L. and Z.Z.; formal analysis, Q.W. and Z.Z.; funding acquisition, Y.S.; investigation, Q.W. and M.L.; methodology, Q.W. and Y.S.; resources, Y.S.; writing—original draft preparation, Q.W.; writing—review and editing, Q.W., M.L., Z.Z. and Y.S. All authors have read and agreed to the published version of the manuscript.

Funding: This research was funded by the Fundamental Research Funds for the Central Universities, grant number 2042021kf0024.

Data Availability Statement: The data presented in this study are available on request from the corresponding author.

Conflicts of Interest: The authors declare no conflict of interest.

References

1. Khonsari, M.M.; Ghatrehsamani, S.; Akbarzadeh, S. On the running-in nature of metallic tribo-components: A review. *Wear* **2021**, *474–475*, 203871. [CrossRef]
2. Yu, X.; Sun, Y.Y.; Wu, S.J. Multi-stage contact model between fractal rough surfaces based on multi-scale asperity deformation. *Appl. Math. Model.* **2022**, *109*, 229–250. [CrossRef]
3. Yu, X.; Sun, Y.Y.; Li, H.G.; Wu, S.J. An improved meshing stiffness calculation algorithm for gear pair involving fractal contact stiffness based on dynamic contact force. *Eur. J. Mech. Solids* **2022**, *94*, 104595. [CrossRef]
4. Liang, X.M.; Wang, G.F. A friction model of fractal rough surfaces accounting for size dependence at nanoscale. *Acta Mech.* **2022**, *233*, 69–81. [CrossRef]
5. Wu, B.Z.; Qin, D.T.; Hu, J.J.; Liu, Y.G. Experimental data mining research on factors influencing friction coefficient of wet clutch. *J. Tribol.* **2021**, *143*, 121802. [CrossRef]
6. Vukelic, D.; Todorovic, P.; Simunovic, K.; Miljojkovic, J.; Simunovic, G.; Budak, I.; Tadic, B. A novel method for determination of kinetic friction coefficient using inclined plane. *Tehnicki Vjesnik—Tech. Gaz.* **2021**, *28*, 447–455.
7. Zhang, X.G.; Zhang, Y.L. Numerical investigation of sliding friction behaviour and mechanism of engineering surfaces. *Ind. Lubr. Tribol.* **2019**, *71*, 205–211. [CrossRef]
8. Zhang, Z.G.; Zou, L.; Liu, H.; Chen, Y.L.; Zhang, B.Z. Simulation and modeling of dynamic friction coefficient of wet clutch during engagement. *Int. J. Automot. Technol.* **2022**, *23*, 125–134. [CrossRef]
9. Kraus, M.; Lenzen, M.; Merklein, M. Contact pressure-dependent friction characterization by using a single sheet metal compression test. *Wear* **2021**, *476*, 203679. [CrossRef]
10. Zhou, C.J.; Hu, B.; Qian, X.L.; Han, X. A novel prediction method for gear friction coefficients based on a computational inverse technique. *Tribol. Int.* **2018**, *127*, 200–208. [CrossRef]
11. Ghatrehsamani, S.; Akbarzadeh, S.; Khonsari, M.M. Experimentally verified prediction of friction coefficient and wear rate during running-in dry contact. *Tribol. Int.* **2022**, *170*, 107508. [CrossRef]
12. Li, G.A.; Hao, S.J.; Gao, W.L.; Lu, Z. The effect of applied load and rotation speed on wear characteristics of Al-Cu-Li alloy. *J. Mater. Eng. Perform.* **2022**, *31*, 5875–5885. [CrossRef]
13. Pan, R.; Zhong, B.; Chen, D.J.; Wang, Z.Z.; Fan, J.W.; Zhang, C.Y.; Wei, S.N. Modification of tool influence function of bonnet polishing based on interfacial friction coefficient. *Int. J. Mach. Tools Manuf.* **2018**, *124*, 43–52. [CrossRef]
14. Galda, L.; Sep, J.; Olszewski, A.; Zochowski, T. Experimental investigation into surface texture effect on journal bearings performance. *Tribol. Int.* **2019**, *136*, 372–384. [CrossRef]
15. Xu, L.Q.; Lu, Y.H.; Liu, Q.R.; Lin, L.K.; Mu, J.H. Experimental study on frictional pairs of piston pumps. *J. Fail. Anal. Prev.* **2022**, *22*, 738–749. [CrossRef]
16. Xia, J.S.; Zhao, J.; Dou, S.S. Friction characteristics analysis of symmetric aluminum alloy parts in warm forming process. *Symmetry* **2022**, *14*, 166. [CrossRef]
17. Wang, W.R.; Zhao, Y.Z.; Wang, Z.M.; Hua, M.; Wei, X.C. A study on variable friction model in sheet metal forming with advanced high strength steels. *Tribol. Int.* **2016**, *93*, 17–28. [CrossRef]
18. Pei, X.; Pu, W.; Zhang, Y.; Huang, L. Surface topography and friction coefficient evolution during sliding wear in a mixed lubricated rolling-sliding contact. *Tribol. Int.* **2019**, *137*, 303–312. [CrossRef]
19. Liang, G.X.; Schmauder, S.; Lyu, M.; Schneider, Y.L.; Zhang, C.; Han, Y. An Investigation of the Influence of Initial Roughness on the Friction and Wear Behavior of Ground Surfaces. *Materials* **2018**, *11*, 237. [CrossRef] [PubMed]
20. Dzierwa, A. Influence of surface preparation on surface topography and tribological behaviours. *Arch. Civ. Mech. Eng.* **2017**, *17*, 502–510. [CrossRef]
21. Sedlaček, M.; Podgornik, B.; Vižintin, J. Influence of surface preparation on roughness parameters, friction and wear. *Wear* **2009**, *266*, 482–487. [CrossRef]
22. Zhang, X.G.; Zhang, Y.L.; Wang, J.M.; Sheng, C.X.; Li, Z.X. Prediction of sliding friction coefficient based on a novel hybrid molecular-mechanical model. *J. Nanosci. Nanotechnol.* **2018**, *18*, 5551–5557. [CrossRef] [PubMed]
23. Wang, Z.S.; Li, S.H.; Sun, J.; Wang, J.H.; Wang, Y.H.; Xia, Z.X.; Wei, C. Experimental study on the effect of load and rotation speed on dry sliding of silicon nitride. *Ind. Lubr. Tribol.* **2021**, *73*, 809–816. [CrossRef]